Laterally mobile, functionalized self-assembled monolayers at the fluorous-aqueous interface in a plug based microfluidic system: characterization and testing with membrane protein crystallization

Jason E. Kreutz, Liang Li, L. Spencer Roach, Takuji Hatakeyama, Rustem F. Ismagilov*

Department of Chemistry, The University of Chicago,929 East 57th Street, Chicago, Illinois 60637
E-mail: r-ismagilov@uchicago.edu

Supporting Information

Chemicals and Materials

All solvents and salts purchased from commercial sources were used as received unless otherwise stated. Tris(hydroxymethyl)aminomethane (Tris base) was obtained from Fisher Scientific. Poly(dimethylsiloxane) (PDMS, Sylgard 184 Silicone Elastomer kit) was obtained from Dow Corning. FC-84 (perfluoroheptane), FC-40 (a mixture of perfluoro-tri-n-butylamine and perfluoro-di-n-butylmethylamine), and FC-70 (Perfluoro- tri-n-pentylamine) were obtained from 3M. Teflon capillaries (OD 250 μm, ID 200 μm and OD 150 μM, ID 50 μM) were received from Zeus Inc. Thirty-gauge Teflon tubing was obtained from Weico Wire & Cable. Gastight syringes were obtained from Hamilton Company. 6-histidine-tagged reaction center (hRC) from *Rhodobacter sphaeroides* was generously provided by Phil Laible of Argonne National Lab. A peptide of 10 histidines tagged with fluorescein (His10) was purchased from Anaspec. 6-histidine-tagged streptavidin (hSA) was purchased from ProSpec-Tany TechnoGene Ltd.

RfOEG synthesis

The synthesis is based on previously published methods.[1] Triethylene glycol (Acros, MW: 150.17) was dried over molecular sieves and 1 equivalent was added to a dried round bottom flask with a stir bar. 1.5 equivalents of $CF_3(CF_2)_7CH_2OH$ (Sigma-Aldrich, MW: 450.1) and 1.3 equivalents of 1,1'-azodicarbonyldipiperidine (ADDP) (TCI, MW: 252.31) were also added to the flask. These were dissolved in anhydrous benzene (Sigma-Aldrich), so that concentrations wee around 0.1 M. The reaction mixture was then stirred and heated to ~ 60 °C. Then 1.4 equivalents of tributylphosphine (Sigma-Aldrich, MW: 202.32) were added to benzene (about half the volume that was added to the round bottom flask) by using an addition funnel. This solution was then slowly added to the reaction mixture over 1-2 hours. Once addition was complete, the mixture was heated for an additional 3 hours, or until color was lost. Upon cooling, a significant amount of precipitant formed. The precipitant was filtered off, and the solvent was removed by rotary-evaporation. Next, the crude product was rinsed and filtered with cold ethyl acetate, the solvent was removed by rotary-evaporation, and the process was repeated in cold methanol to remove all solid impurities. The product was then purified by using column chromatography and fluorous chromatography (Fluorous Technologies). Spectral data: ^{1}H NMR ($CDCl_3$) δ: 3.98 (t, 2H), 3.74 (t, 2H), 3.67 (t, 2H), 3.62 (m, 6H), 3.55 (t, 2H), 3.0 (b, 1H); ^{13}C NMR ($CDCl_3$) δ: 120-105, 72.65, 72.44, 70.86, 70.64, 70.43, 68.35 (t, J = 100 Hz), 61. 73. Electrospray mass spectrometry in positive mode showed a single peak at 583.0 m/z corresponding to $[RFOEG + H^+]^+$.

RfNTA synthesis

Scheme S1 shows the synthetic route to RfNTA **(4)**

Synthesis of $RfOEG_{(6)}$ (1)

Hexaethylene glycol (Sigma-Aldrich, MW: 282.33) was dried over molecular sieves and 1 equivalent was added to a dried round bottom flask with stir bar. 2.5 equivalents of $CF_3(CF_2)_7CH_2OH$ (Sigma-Aldrich, MW: 450.1) and 1.5 equivalents of 1,1'-azodicarbonyldipiperidine (ADDP) (TCI, MW: 252.31) were also added to the flask. These were dissolved in anhydrous benzene (so that concentrations were around 0.1 M). The reaction mixture was then stirred at room temperature. Next, 1.6 equivalents of tributylphosphine (Sigma-Aldrich, MW: 202.32) were dissolved in benzene (about half the volume that was added to the round bottom flask) by using an addition funnel. This solution was then slowly added to the reaction mixture over 3-4 hours, and the reaction was allowed to run overnight. Next, the precipitant was filtered off, and the solvent was removed by rotary-evaporation. The crude product was then rinsed and filtered with cold ethyl acetate, the solvent was removed by rotary-evaporation, and the process was repeated in cold methanol to remove all solid impurities. The product **(1)** was then further purified by using column chromatography and fluorous chromatography. Spectral data: ^{1}H NMR ($CDCl_3$) δ: 4.02 (t, 2H), 3.74 (t, 2H), 3.68 (t, 2H), 3.61 (m, 18H), 3.56 (t, 2H), 3.0 (b, 1H); ^{13}C NMR ($CDCl_3$) δ: 120-105, 72.65, 72.37, 70.76, 70.72, 70.67-70.59, 70.37, 68.33 (t, J = 100 Hz), 61.73. Electrospray mass spectrometry in positive mode showed a single peak at 715.0 m/z corresponding to $[\mathbf{(1)} + H^+]^+$.

Synthesis of (2)

2 equivalents of 1,1'-carbonyldiimidazole (Sigma-Aldrich, MW: 162.15) were dissolved in dry methylene chloride (Fisher). **(1)** (MW: 714.41) was also dissolved in dry methylene chloride and added slowly to the 1,1'-carbonyldiimidazole. The reaction was stirred overnight at room temperature under dry nitrogen. The product **(2)** was purified by using column chromatography. Spectral data: ^{1}H NMR (CD_3OD) δ: 8.33 (s, 1H), 7.63 (s, 1H), 7.09 (s, 1H), 4.1 (t, 2H), 3.88, (m, 2H), 3.78 (m, 2H), 3.61 (m, 20H), 2.0 (b, 1H).

Synthesis of RfNTA (4)

10 equivalents of 1,8-Diazabicyclo[5.4.0]undec-7-ene (Acros, MW: 152.24) and 1 equivalent of Nα,Nα-Bis(carboxymethyl)-L-lysine trifluoroacetate salt **(3)** (Sigma-Aldrich, MW:376.3) were suspended in dry methylene chloride. Next **(2)** (MW: 808.5) was dissolved in methylene chloride and added to the reaction mixture, and then the reaction was stirred overnight at room temperature under dry nitrogen. The solvent was then removed and the remaining solid was washed several times with ethyl acetate. Next, the solid was dissolved in a minimal amount of methanol (Fisher) and sodium isopropylphenoxide (prepared by mixing sodium methoxide (Acros) with a slight excess of isopropylphenol (Sigma-Aldrich)) was added. The mixture was stirred for 15 minutes, and any solid was filtered off. Next, the liquid was evaporated, the solid was dissolved in a minimal amount of methanol, and the product was precipitated using ether (Fisher). The product **(4)** (MW= 1068.6) was then further purified by using fluorous chromatography. Spectral data: ^{1}H NMR (CD_3OD) δ: 4.1 (m, 4H), 3.7 (m, 5H), 3.61 (m, 22H), 3.10 (m, 2H), 2.0-1.5 (m, 6H); ^{13}C NMR ($CDCl_3$) δ: 158.94, 129.93, 73.165, 71.49-71.28, 70.85, 69.31, 68.97 (t, J:= 100 Hz), 64.85, 56.86, 41.28, 30.52, 28.43, 25,48. Electrospray mass spectrometry in negative mode showed a predominant peak at 1000.8 m/z, and an additional peak at 1023.8 m/z consistent with $[RfNTA\text{-}3Na^+ + 2H^+]^-$ salt and $[RfNTA\text{-}2Na^+ + H^+]^-$ respectively.

Characterization
^{1}H and ^{13}C NMR were acquired on Bruker Avance DRX 400MHz or Bruker Avance III 500MHz spectrometers (Bruker BioSpin). ESI-MS were acquired from Agilent 1100 LC/MSD with ESI or APCI ion sources (Agilent Technologies).

PDMS Device Fabrication.
Poly(dimethylsiloxane) (PDMS) was used to fabricate all microfluidic devices. Microchannels with rectangular cross-sections were fabricated with rapid prototyping.[2] The hybrid microfluidic devices consisted of PDMS microchannels (cross-section: 250 μm by 250 μm) with three or four tapered inlets (100 μm by 250 μm) for aqueous phases and one orthogonal inlet for carrier fluid to form plugs of nanoliter volumes. The channel walls were functionalized with (tridecafluoro1,1,2,2-tetrahydrooctyl)-1-trichlorosilane (United Chemical Technologies) to render them hydrophobic and fluorophilic.[3] Teflon tubing was inserted into the outlet up to the junction at which plugs formed. The tubing was sealed to the device with either wax or PDMS glue (Dow-Corning Sylgard).

Interfacial adsorption experiments using hGFP
Microfluidic devices with three aqueous-inlets were used to perform interfacial adsorption experiments. In these experiments, the left aqueous stream contained the additive solution, which was either 1) 100 mM Tris, pH 7.0, 2) 115 μM $NiSO_4$ in 100 mM Tris, pH 7.0, 3) 125 μM RfNTA in 100 mM Tris, pH 7.0, 4) 125 μM **(3)** and 115 μM $NiSO_4$ in 100 mM Tris, pH 7.0, or 5) 62.5 μM RfNTA and 57.5 μM $NiSO_4$ in 100 mM Tris, pH 7.0. The stock buffer solution had been pretreated with chelex to remove any divalent cations, and all other solutions were made from this stock solution. When mixed with RfNTA, the concentration of Ni^{2+} was always between 90-95% of the RfNTA concentration to ensure that no free Ni^{2+} was left in solution. Higher concentrations of RfNTA:Ni were also tested and performed similarly. The center stream always contained 100 mM Tris, pH 7.0, except for the experiment with 20 mM EDTA (Fisher) in 100 mM Tris, pH 7.0. The right stream contained 2 μM hGFP (Upstate, now part of Millipore) and 0.25% lauryldimethylamine *N*-oxide (LDAO) (Anatrace) (w/v) in 100 mM Tris, pH 7.0. Plugs were formed in Teflon tubing (OD 150 μm, ID 50 μm) using FC-40 that had been pre-equilibrated with 20 mM EDTA. The carrier fluid was flowed at a rate of 8.3-16.67 nL/sec, by using PHD2000 syringe pumps (Harvard Apparatus). No additional surfactant was used in the FC-40, except when 0.25 mg/mL RfOEG (MW 582.25) was used. The hGFP always flowed at a rate of 3.33 nL/sec, so the final concentration was 400 nM hGFP and 0.05% LDAO. The other two flow rates were adjusted so that the total aqueous flow rate was always 16.67 nL/sec. The additive and buffer flow rates were both 6.67 nL/sec for additive conditions 1-4, so the final concentrations were 46 μM Ni^{2+}, 50 μM RfNTA, and 50 μM **(3)** and 46 μM Ni^{2+}, for conditions 2-4 respectively. For condition 5, the flow rates were 3.33 and 10 nL/sec for the additive and buffer stream, respectively, leading to final concentrations of 12.5 μM RfNTA and 11.5 μM Ni^{2+}. When EDTA was added to the buffer stream, it gave a final concentration of 12 mM EDTA. Plugs were formed for at least 2 minutes, after which flow was stopped, and then the tubing was cut, and the ends of the tubing were sealed onto a glass slide with wax. For imaging the tubing was submerged in milliQ-H_2O. Bright field and fluorescence images were obtained by using confocal microscopy on a Leica DMI6000 microscope (Leica Microsystems) using a VT-Infinity 3 confocal scanning head (VisiTech international). Images were analyzed using

SimplePCI software (Hammamatsu Corp.) and MetaMorph 6.3 (Molecular Devices). See Figure 1e-g and Figure S2.

FRAP experiments

Plugs were formed as described above. The final concentration of His10 was 3.7 μM in 20 mM Tris pH 8.0. The final RfNTA:Ni concentration was 30 μM RfNTA and 28.5 μM Ni. Plugs were formed in three different fluorocarbons: FC-70 with a viscosity of 12 cSt, FC-40 with a viscosity of 1.8 cSt, and FC-84 with a viscosity of 0.53 cSt at room temperature. All fluorocarbons contained 170 μM RfOEG to prevent nonspecific adsorption.

During the FRAP experiments 10 images of the edges of a plug were obtained before bleaching. Next, spots were bleached on the edges of the plugs using high laser power for 2 seconds, and the regions were then monitored for an additional 40 seconds. Linescans spanning the edges of the plugs were used to monitor fluorescence recovery at the plug interface over time. The shape of the bleach spot was fit using Origin 8 (OriginLab) to the Gaussian curve described by Equation 1. A generalized solution to Fick's second law of diffusion is given in Equation 2 and draws obvious parallels to Equation 1.[4]

Equation 1: $$I(x,t) = I_0 - A(t) * e^{\frac{-(x-x_0)^2}{2*w^2}}$$

Equation 2: $$C(r,t) = C_0 - \frac{M}{(4\pi Dt)^{d/2}} * e^{\frac{-r^2}{4Dt}}$$

I is intensity, I_0 is the initial intensity, A(t) is the maximum amplitude at time t, x is the position, and x_0 is the offset, and w determines the distribution width of the curve. C is the concentration, C_0 is the initial concentration. M is the total amount of the diffusing species, D is the diffusion coefficient, r is the position, and t is time.

Monitoring the change in the shape of the Gaussian over the time course of recovery allows for extraction of a diffusion coefficient and requires no predetermined knowledge of the geometry of the bleach spot or of the diffusion dimension.[4] From Equations 1 and 2 it can be seen that $w^2 = 2*D*t$, so plotting w^2 vs. t should give a straight line with slope 2*D. The diffusion dimension can be determined using $\log A(t) = -d/2 * \log(t) + K$.

This analysis gave diffusion coefficients of 7.3 ± 2.6 x 10^{-12} m^2/sec, 15.2 ± 2.4 x 10^{-12} m^2/sec, 39.2 ± 11.5 x 10^{-12} m^2/sec for FC-70, FC-40 and FC-84 respectively (Figure S4 and Table S1). In all cases there was basically complete recovery of fluorescence indicating that no immobile phase existed. The measured diffusion dimension was 1.1 ± .3, 1.1 ± .2, 2.0 ± .4 for FC-70, FC-40 and FC-84 respectively (Table S1). However, due to the log-log plot, the accuracy of d is greatly affected by the time range in which reliable data can be obtained. Divalent metals are capable of quenching fluorescein, and significant quenching was observed when using His10. This led to fairly noisy data, which limited the timescale over which accurate measurements could be obtained (Figure S3). Analysis including later time points than those shown in Figure S4 indicated that d for FC-70 was likely accurate; whereas d for FC-40 fell between 1 and 2, and d for FC-84 remains near 2. This general trend of increasing diffusion dimension with faster diffusion can be explained if the geometry of the bleaching zone is considered. The bleaching zone is not a point; rather, there is a cone above and below the focal plane. If the bleaching zone of the laser above and below the focal plane is large compared to the length scale of diffusion, then the predicted diffusion dimension would be 1, as recovery can

only come from fluorophore in the focal plane. On the other hand, for faster diffusion, the diffusion dimension would approach 2 as fluorophores above and below the plane could contribute.

Similar experiments were performed with hGFP at 1 μM, and fluorescein-labeled hSA at 250 nM. The hGFP could not be analyzed in the same fashion due to a quenching effect that resulted in a temporary enhancement of fluorescence around the bleach spot during recovery (Figure S5). Rough estimates of D_0, obtained by fitting fluorescence recovery of the area surrounding the bleach spot with a single exponential curve, were approximately 3 x 10^{-12} m^2/sec for FC-40 and 30 μM RfNTA:Ni. For the labeled hSA interfacial binding was weak, possibly due to the close proximity of the his-tag to structural components of the protein. However, initial experiments resulted in D_0 using the Gaussian fitting model of 4.5 ± 0.6 and 9.2 ± 2.4 x 10^{-12} m^2/sec for FC-70 and FC-40, respectively (Table S1). It makes sense that the hGFP and hSA give slower diffusion than His10, as a protein would create more drag than a small peptide. However the D_0 for a protein in solution is around 1 x 10^{-10} m^2/sec, so events at the interface still dominate the diffusion rather than the attached protein or peptide.

FRAP was measured using a Leica tandem scanner SP5 spectral confocal on a DMI6000 microscope with a 40x NA1.40 oil objective. Images were analyzed by using ImageJ software and the plug-in loci bio-formats and by using Mathematica. See Figures 1h, S3, S4, S5 and Table S1.

Tensiometry

Droplets of the solution of fluorous surfactant were formed at the end of disposable droplet extrusion tips. The tips were assembled by using quick-set epoxy to glue polyimide-coated glass tubing into 1-10μL disposable pipet tips that were oxidized in a Plasma Prep II plasma cleaner (SPI Supplies) for 1.5 minutes to render them hydrophilic. The end of the capillary was positioned just inside the end of the pipet tip. The polyimide tubing was connected to a 50 μL Hamilton Gastight syringe by using 30-gauge Teflon tubing. The syringe was then filled with the fluorous solution. The pipette tip was positioned so that it sat in the aqueous solution within a 1 mL polystyrene cuvette, and the tip was held in place by a clamp. The formed droplets were imaged using Model 250 Standard Digital Goniometer & DROPimage Advanced software (Rame-Hart Instrument Co). See Figure S1.

Crystallization of his-tagged reaction center (hRC). For each of the six different additive conditions, two sets of 40 individual crystallization trials were set up for each of the five precipitant concentrations. Four-aqueous-inlet devices were used to perform crystallization experiments. In sequence, the precipitant stream was 50% (w/v) PEG 4000, 1.1 M NaCl, 9% (w/v) 1,2,3-heptanetriol (HPT) in 50 mM Tris pH 7.8. The buffer stream was 9% HPT in 50 mM Tris pH 7.8. The additive stream used six different solutions in six different sets of experiments, and they were 1) 10 mM Tris pH 7.8, which was defined as the standard condition, 2) 45 μM $NiSO_4$ in 10 mM Tris pH 7.8, 3) 50 μM RfNTA in 10 mM Tris pH 7.8, 4) 50 μM RfNTA and 45 μM $NiSO_4$ in 10 mM Tris pH 7.8, 5) 200 μM RfNTA and 180 μM $NiSO_4$ in 10 mM Tris pH 7.8, and 6) 200 μM RfNTA and 180 μM $NiSO_4$ and 10 mM imidazole in 10 mM Tris pH 7.8. The protein stream was 6 mg/mL hRC from *Rhodobacter sphaeroides* in 0.05% (w/v) LDAO and 10 mM Tris pH 7.8. The fluorinated carrier fluid was FC-40. The carrier fluid, protein, and additive streams were maintained at constant flow rates of 41.7 nL/sec, 13.3 nL/sec and 3.3 nL/sec, respectively. The flow rate of the precipitant stream was first increased from 8.3 nL/sec to 15

nL/sec, and then decreased from 15 nL/sec to 8.3 nL/sec, with a step size of 1.7 nL/sec. Correspondingly, the buffer stream was first decreased from 8.3 nL/s to 1.7 nL/sec, and then increased from 1.7 nL/sec to 8.3 nL/sec, with a step size of 1.7 nL/sec. Each flow rate step lasted for 14 s. After one step was finished, the subroutine was stopped and, ~5 s later, it was restarted with the setup of the next step. In this experiment, two sets of plugs generated from identical flow rates were counted as duplicates. The experiments were performed six times with six different additive solutions. The trials, in the form of plugs, were transported and stored in Teflon tubing (O.D.: 250 μm and I.D.: 200 μm) which was sealed inside glass tubing (O.D.: 3 mm and I.D.: 1.8 mm) prefilled with FC-70. The experiment was performed under dim light, and the trials were kept in the dark at 23 ^{o}C.

The following final precipitant concentrations were obtained: 0.45 × [ppt]= 22.5% (w/v) PEG 4000, 0.495 M NaCl, 4.5% (w/v) 1,2,3-heptanetriol (HPT) in 30 mM Tris pH 7.8, 0.4 × [ppt]= 20% (w/v) PEG 4000, 0.44 M NaCl, 4.5% (w/v) 1,2,3-heptanetriol (HPT) in 30 mM Tris pH 7.8, 0.35 × [ppt]= 17.5% (w/v) PEG 4000, 0.385 M NaCl, 4.5% (w/v) 1,2,3-heptanetriol (HPT) in 30 mM Tris pH 7.8, 0.3 × [ppt]= 15% (w/v) PEG 4000, 0.33 M NaCl, 4.5% (w/v) 1,2,3-heptanetriol (HPT) in 30 mM Tris pH 7.8, 0.25 × [ppt]= 12.5% (w/v) PEG 4000, 0.275 M NaCl, 4.5% (w/v) 1,2,3-heptanetriol (HPT) in 30 mM Tris pH 7.8. Because the behavior of crystallization can be different depending on the purity of samples, the experiment was performed twice with different protein preparations made months apart, and similar results were obtained both times. To avoid spurious results from background levels of divalent metals such as those observed for condition 3, low levels of a chelating agent such as EDTA could be added to the crystallization conditions. The data presented in this paper is from the current purification protocol performed by Phil Laible of Argonne National Lab.

Counting plugs with crystals. Counting of plugs was performed under dim light, at day 1, day 2, day 5, and day 12 after setting up the experiments. In all experiments for each flow rate step, 40 plugs were counted, starting from the tenth plug of each set. Plugs with crystals were counted as one hit. To make sure we did not start from different plugs on different days, we took a picture of the first counted plug in each set of plugs.

Determining the nucleation rate. The nucleation rate was determined for different additive conditions at two precipitant concentrations: 1) 0.40 × [ppt] where plugs of crystallization trials were formed at 13.3 nL/sec and 2) 0.45 × [ppt] where plugs of crystallization trials were formed at 15 nL/sec. 0.40. In 1) finalconcentrations of precipitant were 20% (w/v) PEG 4000, 0.44 M NaCl and 30 mM Tris pH 7.8, whereas in 2) final concentrations of precipitant were 22.5% (w/v) PEG 4000, 0.5 M NaCl and 30 mM Tris pH 7.8. To determine the nucleation rate for each concentration of precipitant, the percentage of the number of plugs with crystals out of the total number of counted plugs (40 in all cases) was plotted against the recording time (days) (Figure S6). The nucleation rate was then extracted from the slope of the plots, determined by dividing the change in the number of plugs with crystals by the change in time. The nucleation rate was equal to the largest slope for each curve. If no crystals were obtained over time, the nucleation rate was zero. All the nucleation rates were extracted from day 0 to day 1 except the one for the standard condition at 0.45 × [ppt], which was extracted from day 0 to day 5. The nucleation rates were plotted in a histogram in Figure 2b.

In our experiments, we counted the number of plugs instead of the number of crystals. For standard conditions, there was always only one crystal per plug, whereas many of the other

conditions often had multiple crystals per plug. Because the number of individual nucleation events was not counted, the calculated nucleation rates represent the lower limit of the actual nucleation rate.

Crystal preparation and X-ray Data Collection. Cryo-protectant for freezing hRC crystals was 25% (v/v) PEG 400, 20% (w/v) PEG 4000, 0.44 M NaCl in 0.08% (w/v) LDAO and 20 mM Tris pH 7.8. Crystals of hRC from *R. sphaeroides* grown in the plugs were extracted by attaching a syringe to one end of the Teflon tubing and flowing the crystals slowly into a drop of cryo-protectant by using the manual syringe driver.[5] Once crystals were flowed into a 2 μL drop of cryo-protectant, the crystals were picked up with a CryoLoop (Hampton Research) and flash frozen in liquid nitrogen. The X-ray diffraction experiments were performed at GM/CA Cat station 23 ID-B of the Advanced Photon Source (Argonne National Laboratory). In all experiments, the wavelength was kept at 1.03 Å. We used a 10 μm minibeam and set the attenuation at five. The exposure time was kept at 10 seconds. The data were processed in HKL2000[6] to determine space group and diffraction limit with S/N over 2.0. The best diffraction limits for different additive conditions are listed in Table S2. Figure S8 shows some representative diffraction patterns.

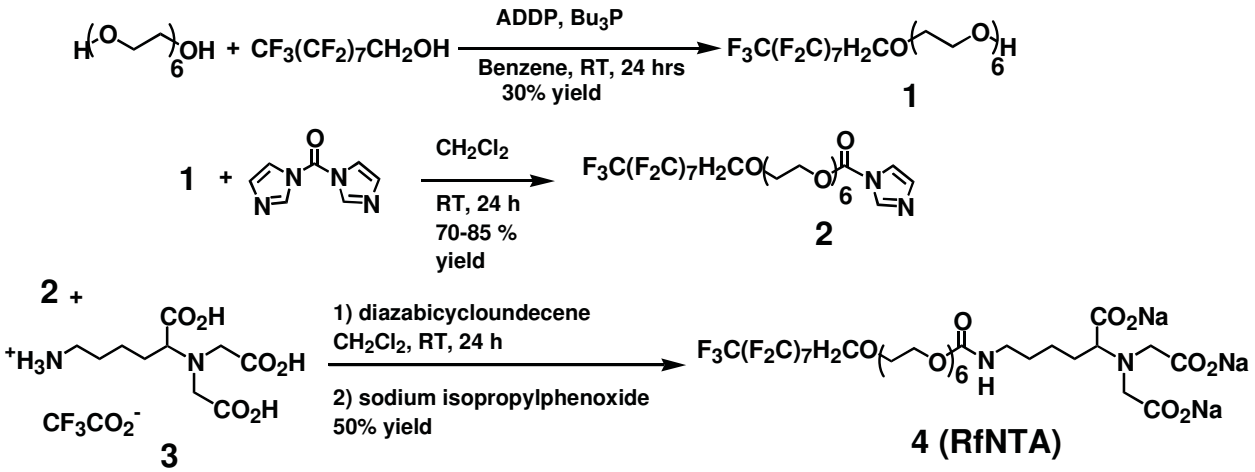

Scheme S1: Synthesis of RfNTA.

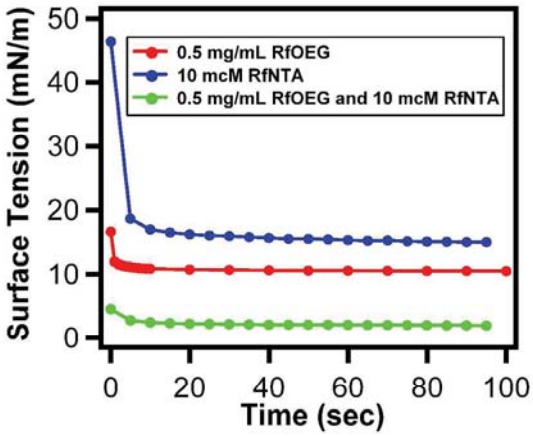

Figure S1: Surface tension measurements of RfOEG and RfNTA alone (red and blue, respectively) and together (green). They coexist at the interface, as indicated by the observation that the surface tension of the combined system is lower than either component individually.

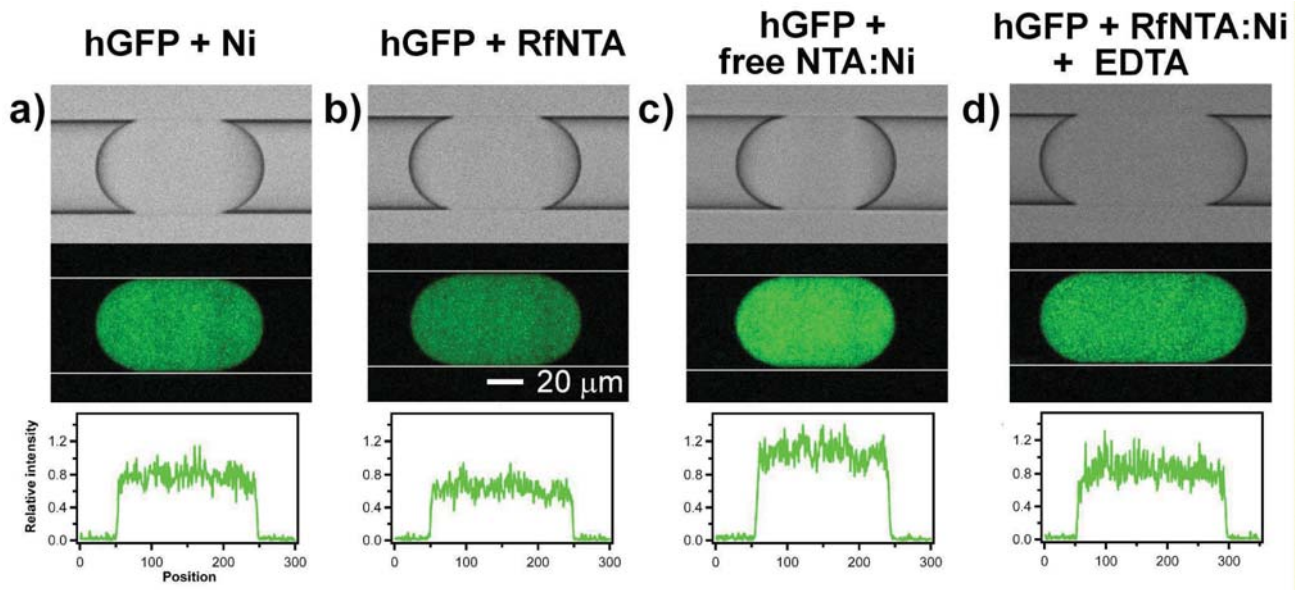

Figure S2: No interfacial adsorption occurs with (a) just Ni^{2+} or (b) just RfNTA. (c) There is also no interfacial adsorption when NTA, with no fluorous tail, + Ni^{2+} is added. (d) The addition of EDTA to an RfNTA:Ni system also prevents any interfacial adsorption by binding up all the Ni^{2+}.

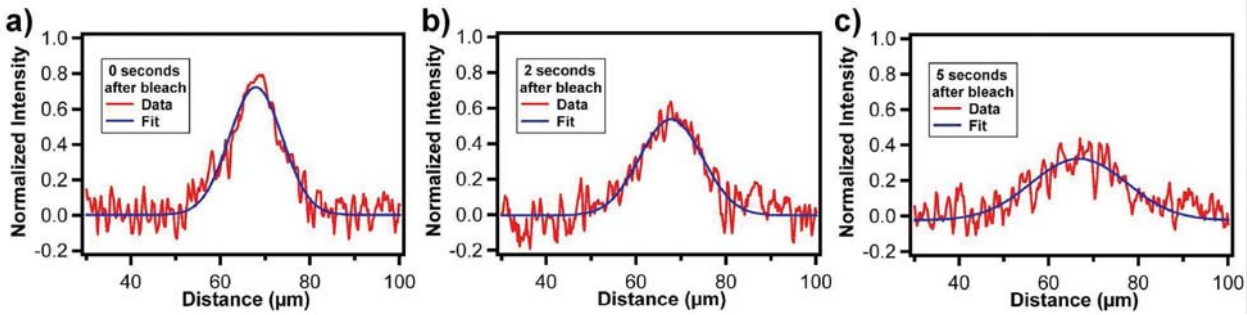

Figure S3: Data and Gaussian fits for images shown in Figure 1h a) from immediately after bleaching, b) from 2 seconds after bleaching and c) from 5 seconds after bleaching.

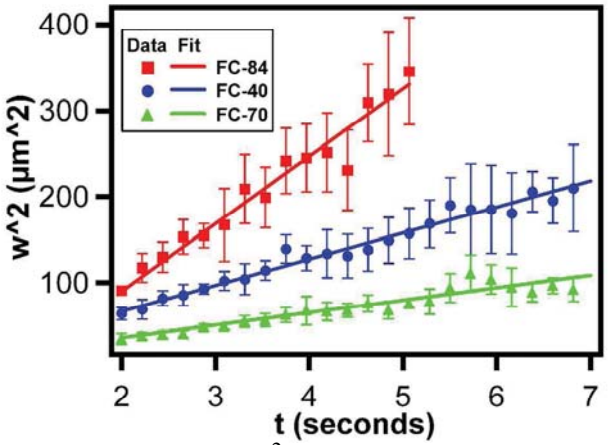

Figure S4: Plot of w^2 vs t from the Gaussian fits of the FRAP data obtained for His10 when the fluorocarbon used was FC-84 (red squares), FC-40 (blue circles) and FC-70 (green triangles). The slope of the fit of these lines was used to determine D_0.

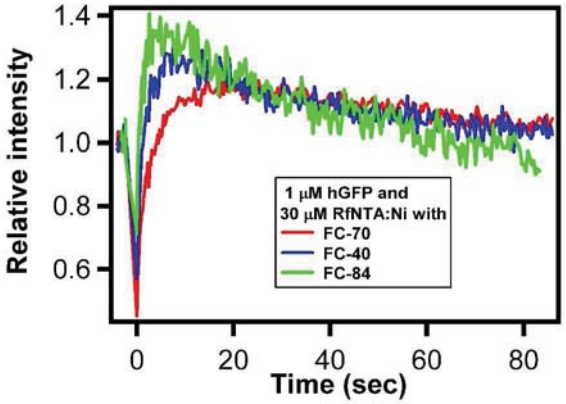

Figure S5: Fluorescence recovery of plugs containing 1 μM hGFP and 30 μM RfNTA:Ni surrounded by fluorocarbons of different viscosities. The temporary fluorescence enhancement shown here would not allow for proper fits to a Gaussian curve, but the recovery rate still shows a dependence on the fluorocarbon used.

	His10				hSA			
Fluoro carbon	D_0 (m^2/sec)	Error (m^2/sec)	d	Error	D_0 (m^2/sec)	Error (m^2/sec)	d	Error
FC-84	39.2 x10^{-12}	11.5 x10^{-12}	2.0	0.4	-	-	-	-
FC-40	15.2 x10^{-12}	2.4 x10^{-12}	1.1	0.2	9.2 x10^{-12}	2.4 x10^{-12}	1.0	0.1
FC-70	7.3 x10^{-12}	2.6 x10^{-12}	1.1	0.3	4.5 x10^{-12}	0.6 x10^{-12}	0.8	0.2

Table S1: Diffusion coefficients and diffusion dimension obtained from FRAP experiments using His10 and hSA. The error represents the 95% confidence interval.

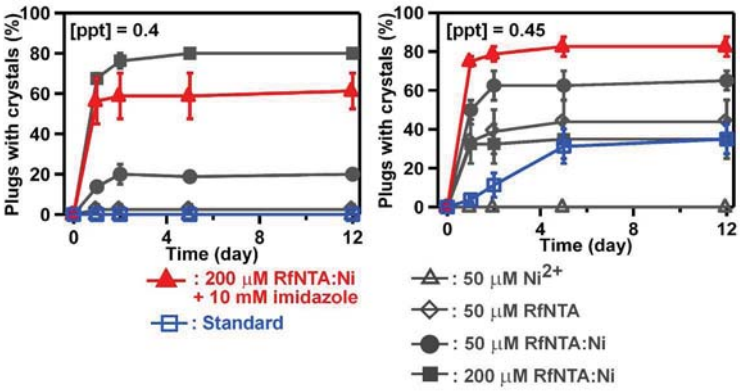

Figure S6: The increase in the number of plugs with crystals of hRC over time. Six different additive conditions were plotted at two precipitant concentrations, 0.4 × [ppt] (left) and 0.45 × [ppt] (right)respectively. The nucleation rates were extracted from the plots and represented in Figure 2b.

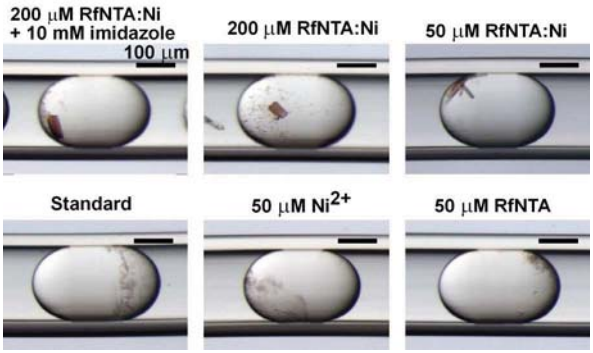

Figure S7: At lower precipitant concentrations (0.35 × [ppt]; 17.5% (w/v) PEG 4000, 0.385 M NaCl, 4.5% (w/v) 1,2,3-heptanetriol (HPT) in 30 mM Tris pH 7.8) hRC crystals were only obtained upon addition of the RfNTA:Ni complex (top row of images).

Condition		X-ray diffraction resolution	Frames collected (0.5 °/frame)	Mosaicity
Standard/45% ppt	Crystal 1	4Å	2	4.0
	Crystal 2	6 Å	2	2.9
50 μm RfNTA /40% ppt	Crystal 1	4.5 Å	1	N/A
	Crystal 2	6 Å	5	6.0
50 μm RfNTA /45% ppt	Crystal 1	4 Å	18	1.2
	Crystal 2	5 Å	2	3
50 μm RfNTA:Ni/35% ppt	Crystal 1	13 Å	1	N/A
	Crystal 2	18 Å	1	N/A
50 μm RfNTA:Ni /40% ppt	Crystal 1	3.7 Å	1	N/A
	Crystal 2	4 Å	1	N/A
50 μm RfNTA:Ni /45% ppt	Crystal 1	3.5 Å	18	3.1
	Crystal 2	3.7 Å	1	N/A
200 μm RfNTA:Ni /30% ppt	Crystal 1	18 Å	1	N/A
	Crystal 2	20 Å	1	N/A
200 μm RfNTA:Ni /35% ppt	Crystal 1	3.5 Å	16	2.0
	Crystal 2	3.5 Å	2	4.0
200μm RfNTA:Ni /40% ppt	Crystal 1	3.1 Å	48	2.5
	Crystal 2	4 Å	14	2.8
200 μm RfNTA:Ni /45% ppt	Crystal 1	over 20 Å	1	N/A
	Crystal 2	over 25 Å	1	N/A
200 μm RfNTA:Ni + imidazole/30% ppt	Crystal 1	7 Å	1	N/A
200 μm RfNTA:Ni + imidazole /35% ppt	Crystal 1	6 Å	1	N/A
	Crystal 2	7 Å	1	N/A
200 μm RfNTA:Ni + imidazole /40% ppt	Crystal 1	3.7 Å	20	3.8
	Crystal 2	8 Å	1	N/A
200 μm RfNTA:Ni + imidazole /45% ppt	Crystal 1	3.5 Å	18	2.4

Table S2: Summary of X-ray diffraction of crystals of hRC in different additive conditions. Data were obtained from two crystals at most conditions

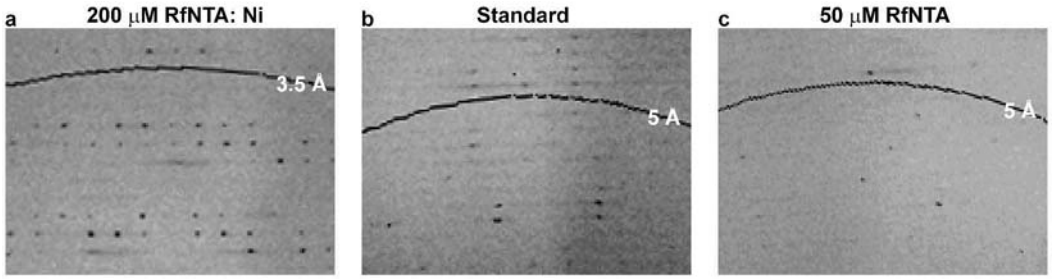

Figure S8: X-ray diffraction of hRC crytals grown in different additive conditions.
a) Crystals from 200 μm RfNTA:Ni at 0.4 × [ppt] diffracted best to 3.1 Å ; b) Crystals from the standard condition at 0.45 × [ppt] diffracted best to 4 Å and c) Crystals from 50 μM RfNTA at 0.45 × [ppt] diffracted best to 4 Å.

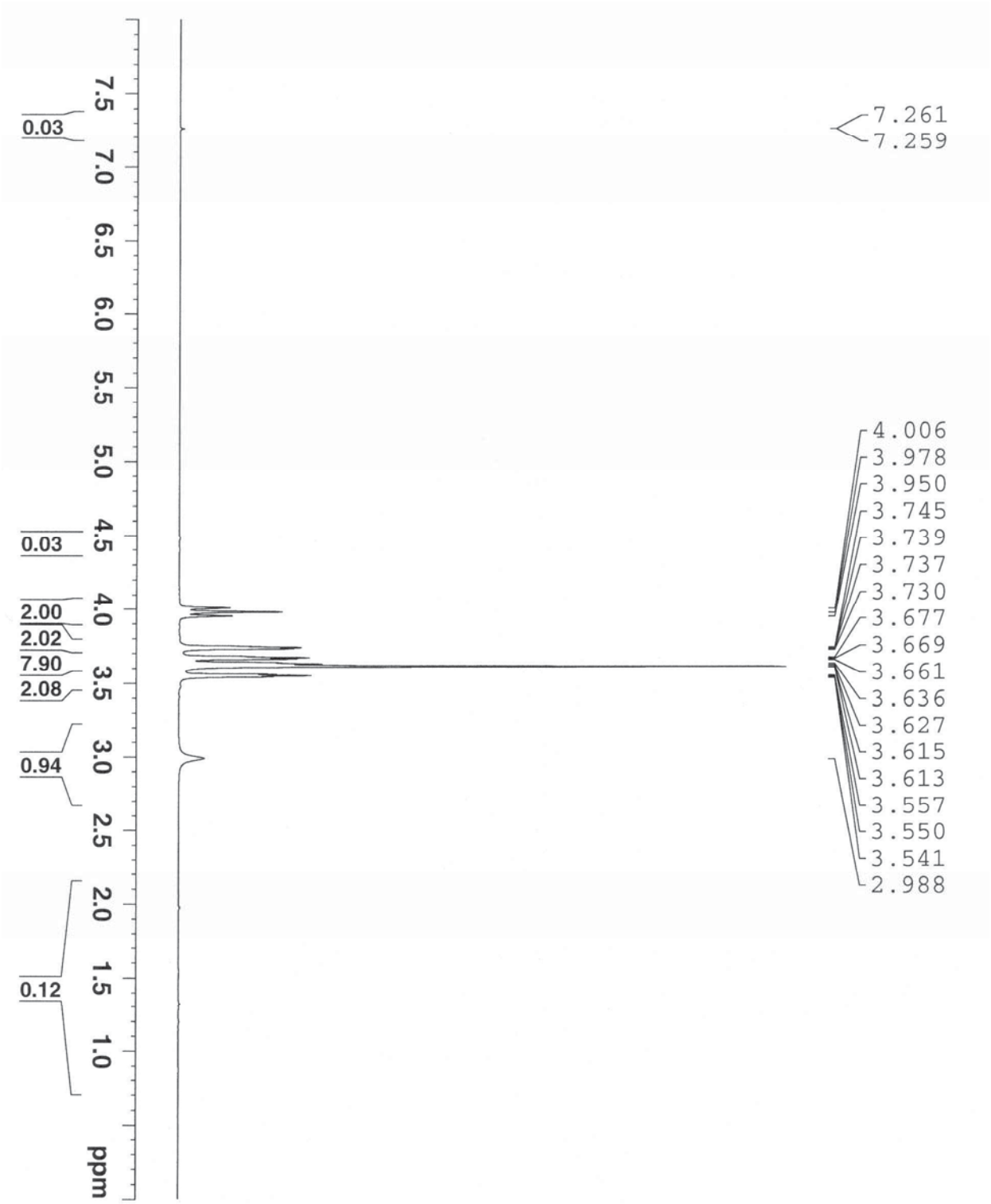

^{1}H NMR of RfOEG

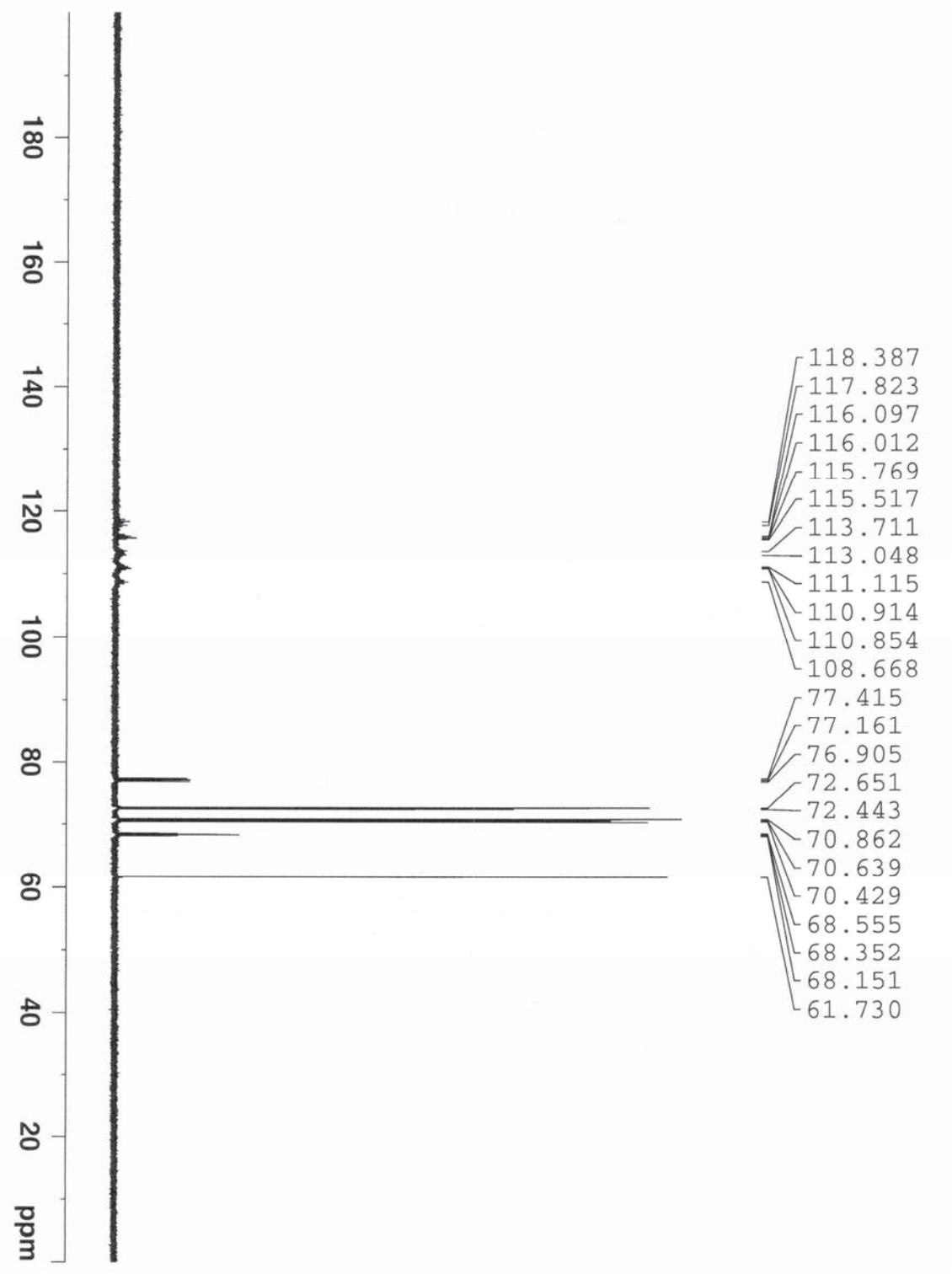

^{13}C NMR of RfOEG

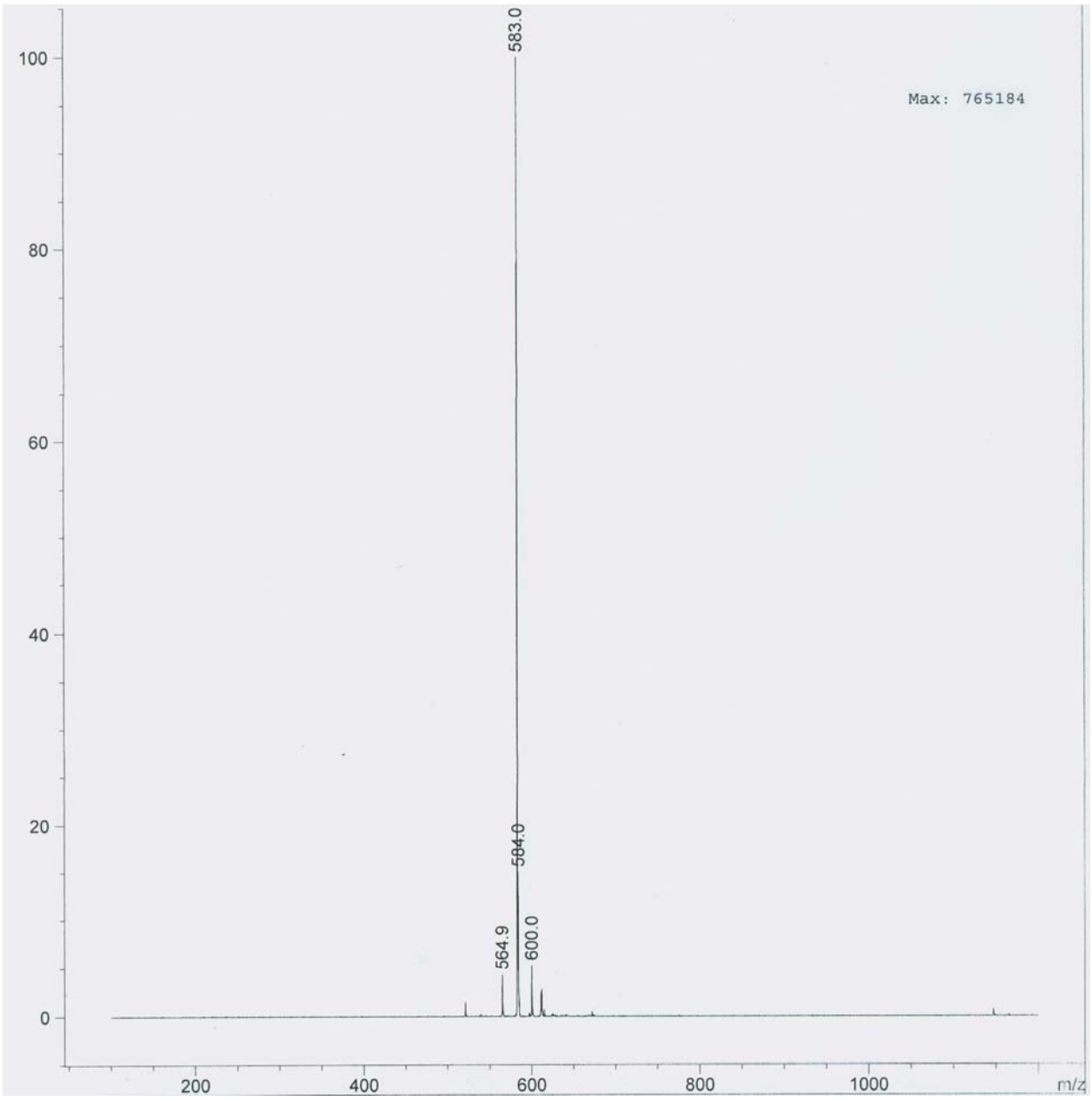
583.0
Max: 765184
100
80
60
40
20
0
584.0
564.9
600.0
200
400
600
800
1000
m/z

MS of RfOEG

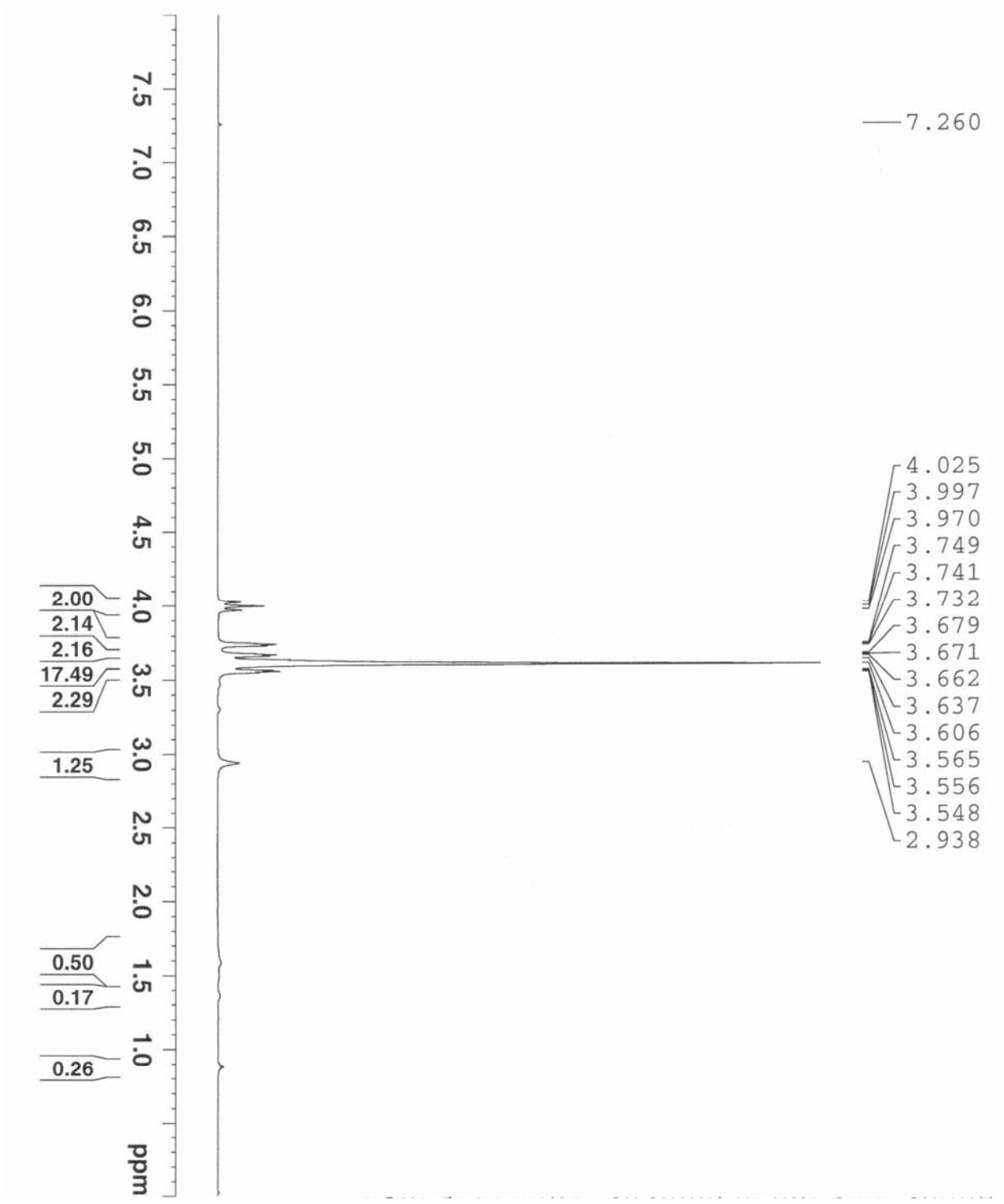
7.260
4.025
3.997
3.970
3.749
3.741
3.732
3.679
3.671
3.662
3.637
3.606
3.565
3.556
3.548
2.938
2.00
2.14
2.16
17.49
2.29
1.25
0.50
0.17
0.26
7.5
7.0
6.5
6.0
5.5
5.0
4.5
4.0
3.5
3.0
2.5
2.0
1.5
1.0
ppm

^{1}H NMR of (1)

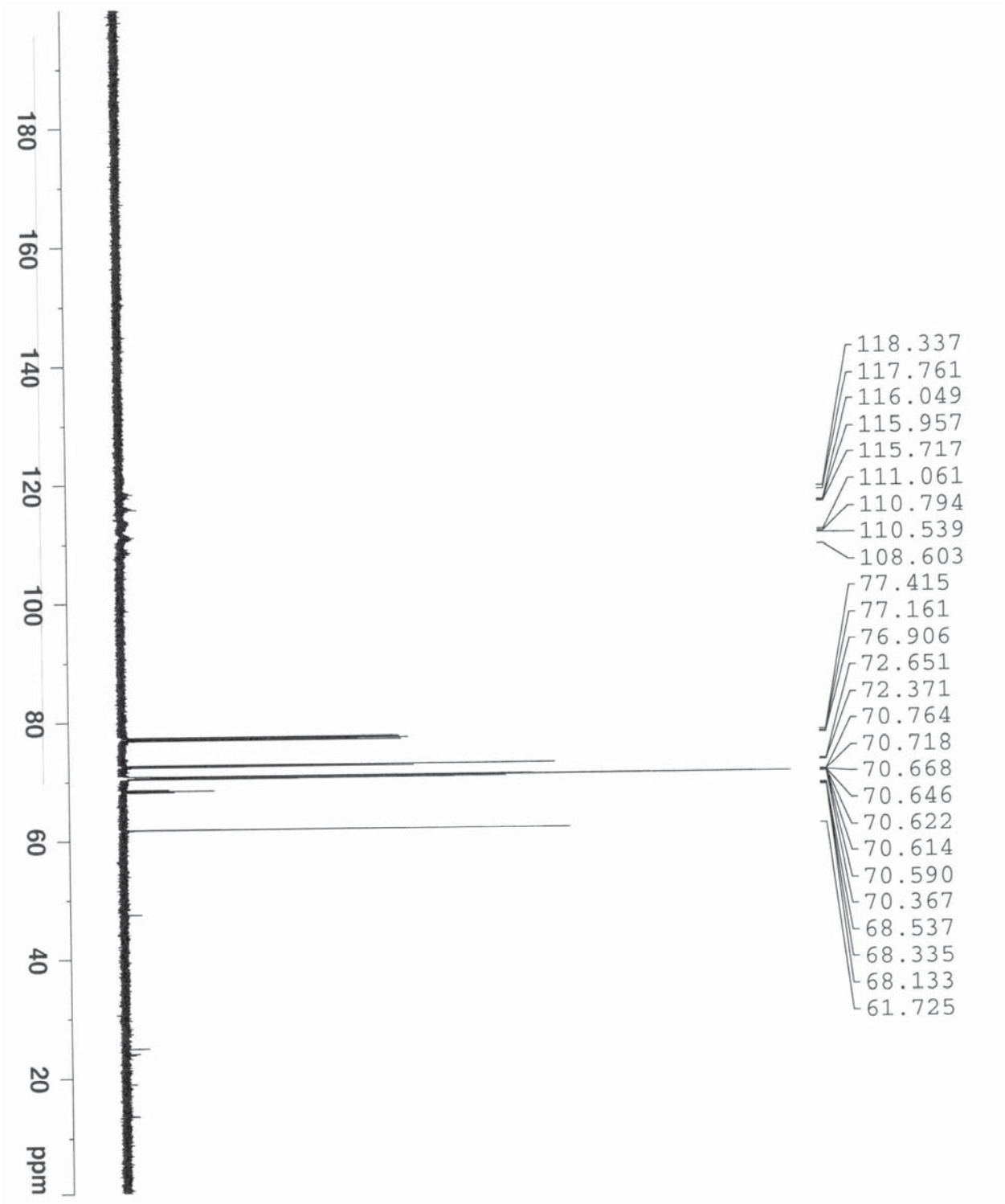
180
160
140
120
100
80
60
40
20
ppm
118.337
117.761
116.049
115.957
115.717
111.061
110.794
110.539
108.603
77.415
77.161
76.906
72.651
72.371
70.764
70.718
70.668
70.646
70.622
70.614
70.590
70.367
68.537
68.335
68.133
61.725

^{13}C NMR of (1)

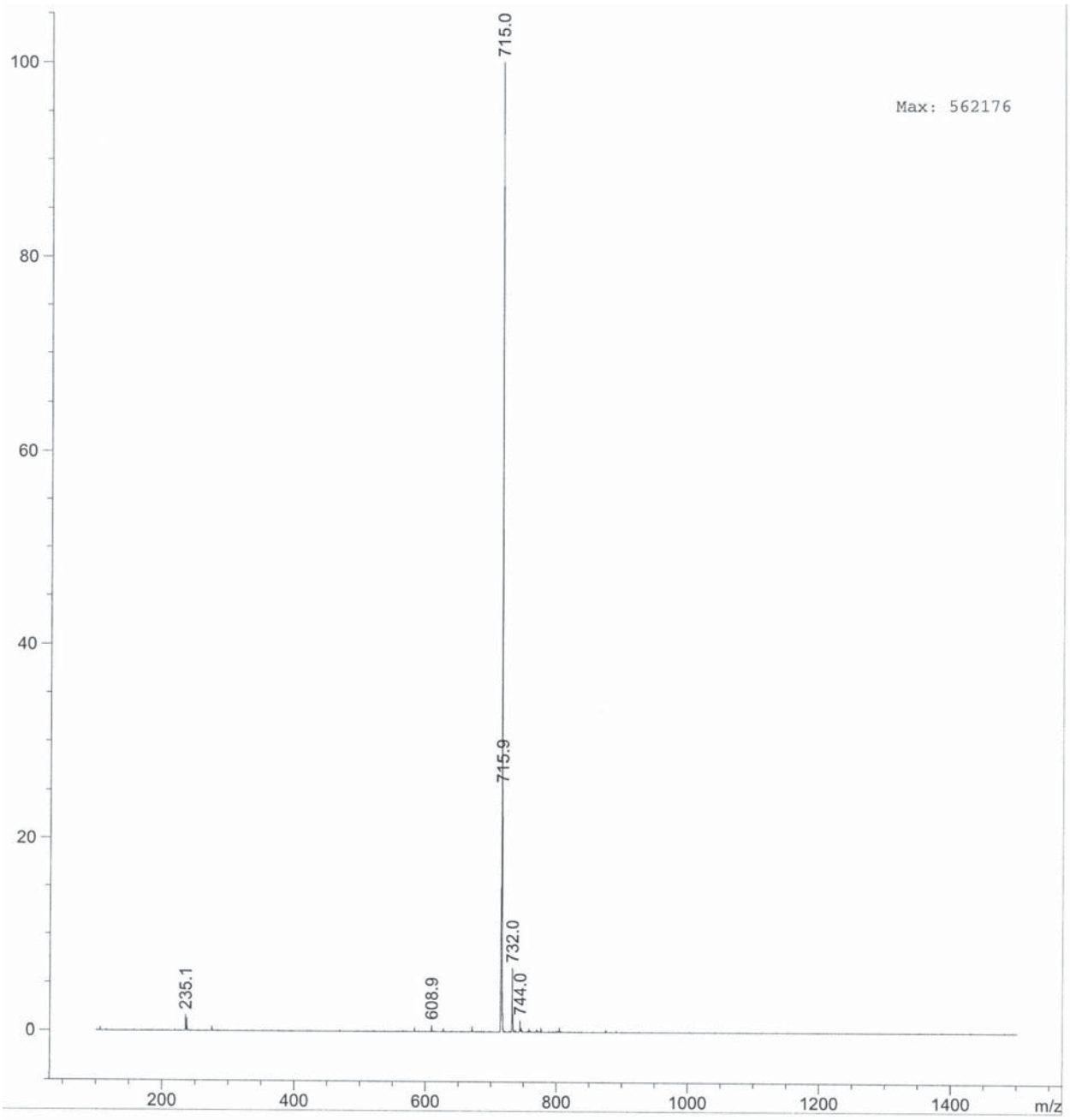
715.0
Max: 562176
100
80
60
40
20
0
715.9
732.0
744.0
235.1
608.9
200
400
600
800
1000
1200
1400
m/z

MS of (1)

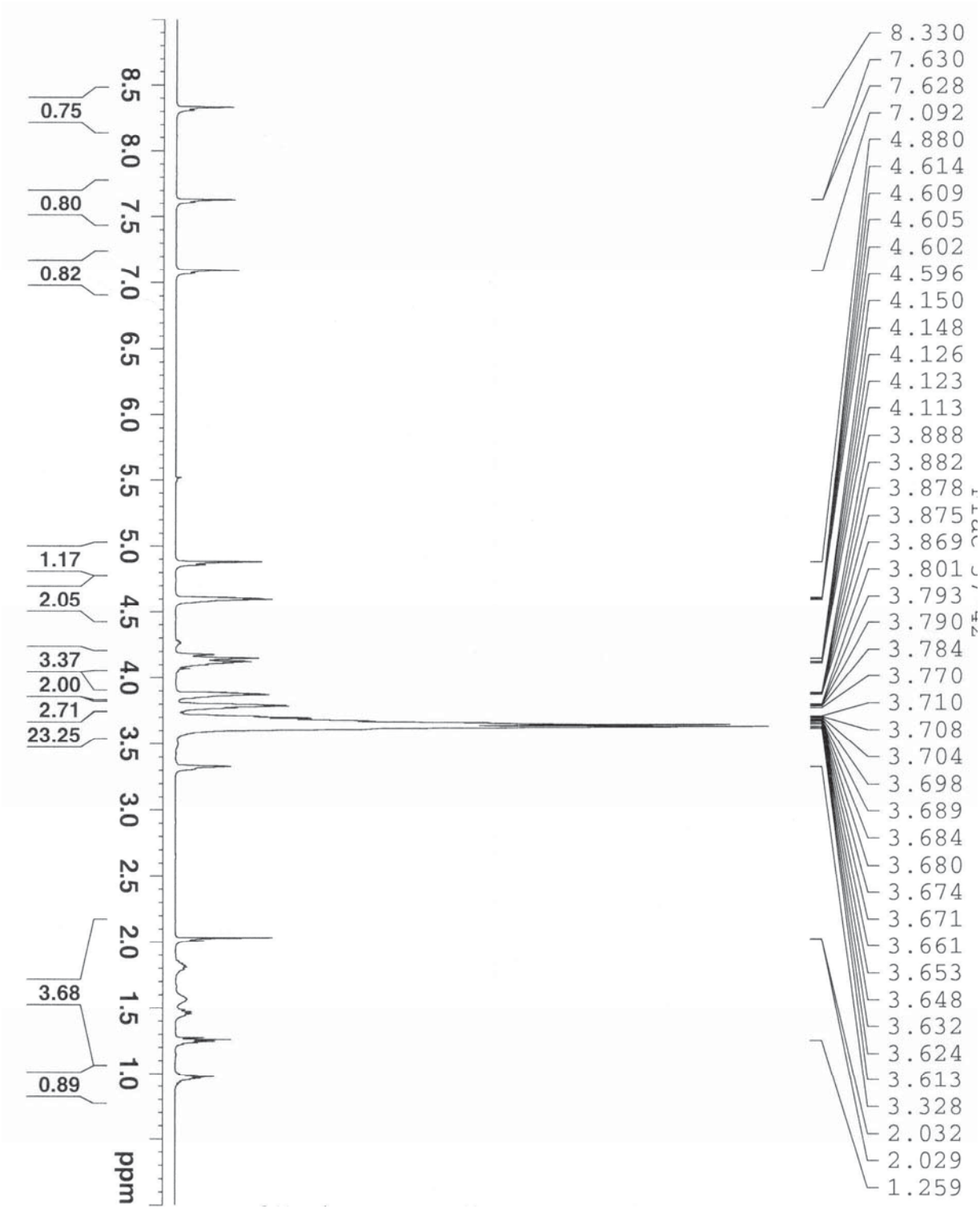
8.330
7.630
7.628
7.092
4.880
4.614
4.609
4.605
4.602
4.596
4.150
4.148
4.126
4.123
4.113
3.888
3.882
3.878
3.875
3.869
3.801
3.793
3.790
3.784
3.770
3.710
3.708
3.704
3.698
3.689
3.684
3.680
3.674
3.671
3.661
3.653
3.648
3.632
3.624
3.613
3.328
2.032
2.029
1.259
0.75
0.80
0.82
1.17
2.05
3.37
2.00
2.71
23.25
3.68
0.89
8.5
8.0
7.5
7.0
6.5
6.0
5.5
5.0
4.5
4.0
3.5
3.0
2.5
2.0
1.5
1.0
ppm

^{1}H NMR of (2)

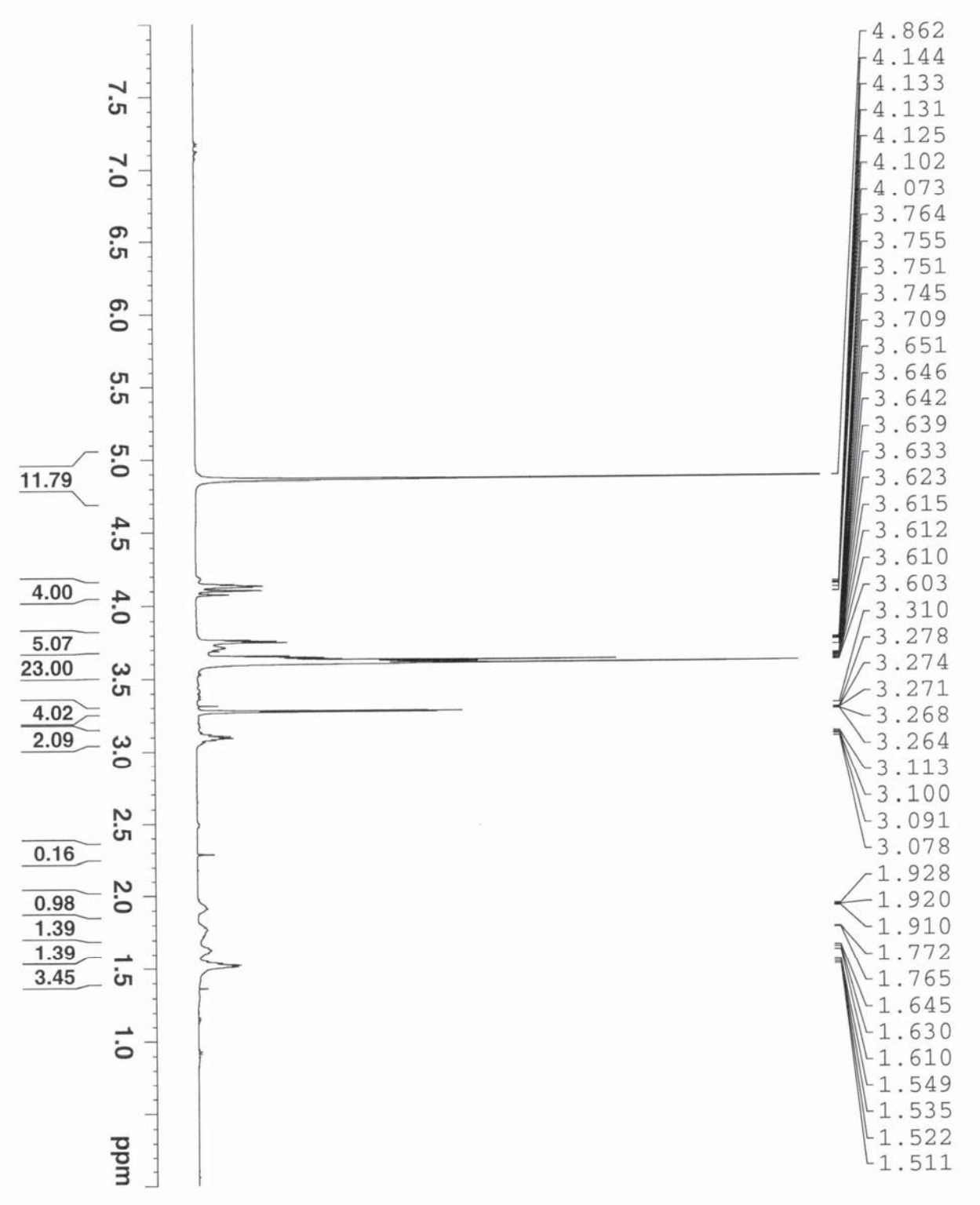

^{1}H NMR of RfNTA

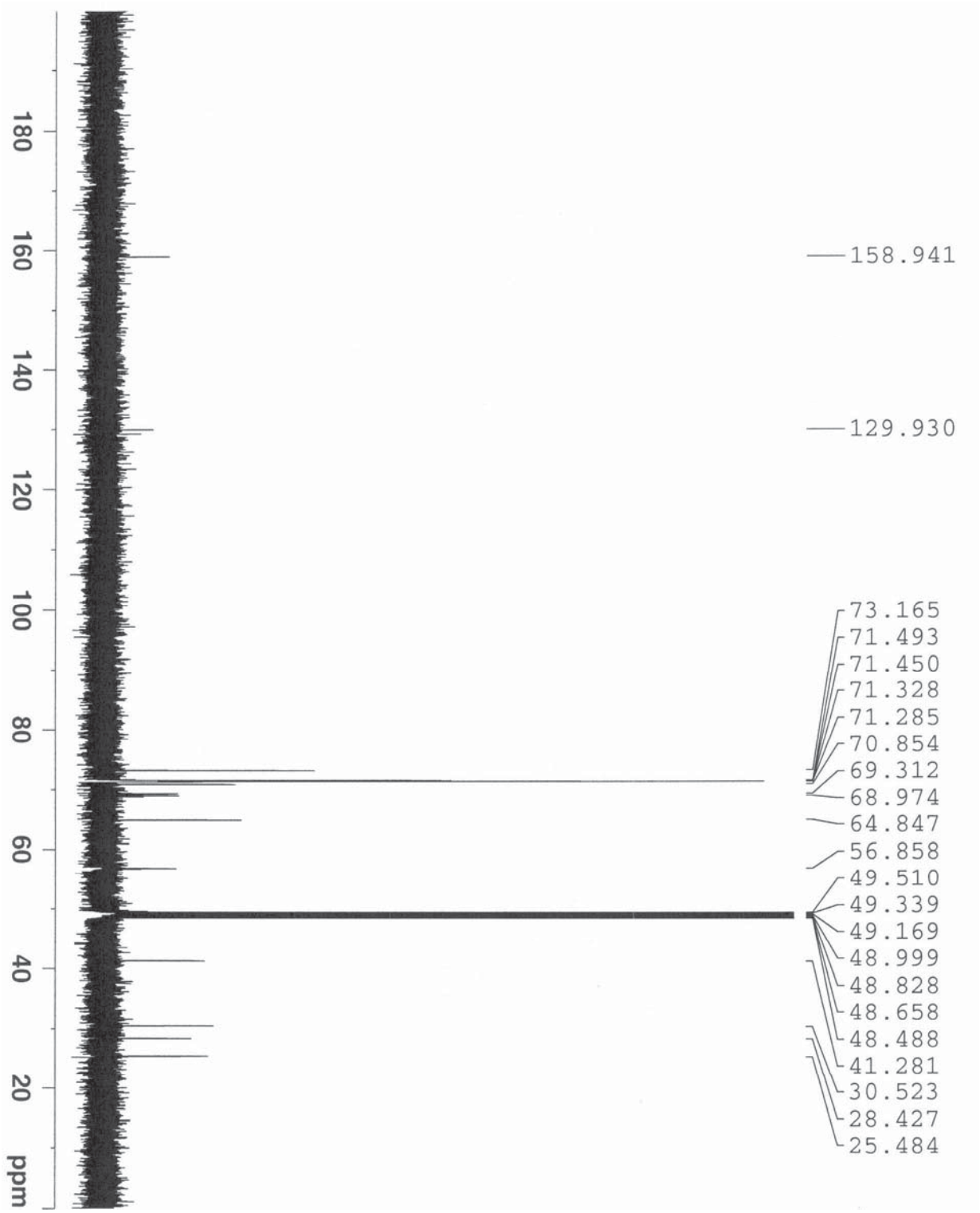

^{13}C NMR of RfNTA

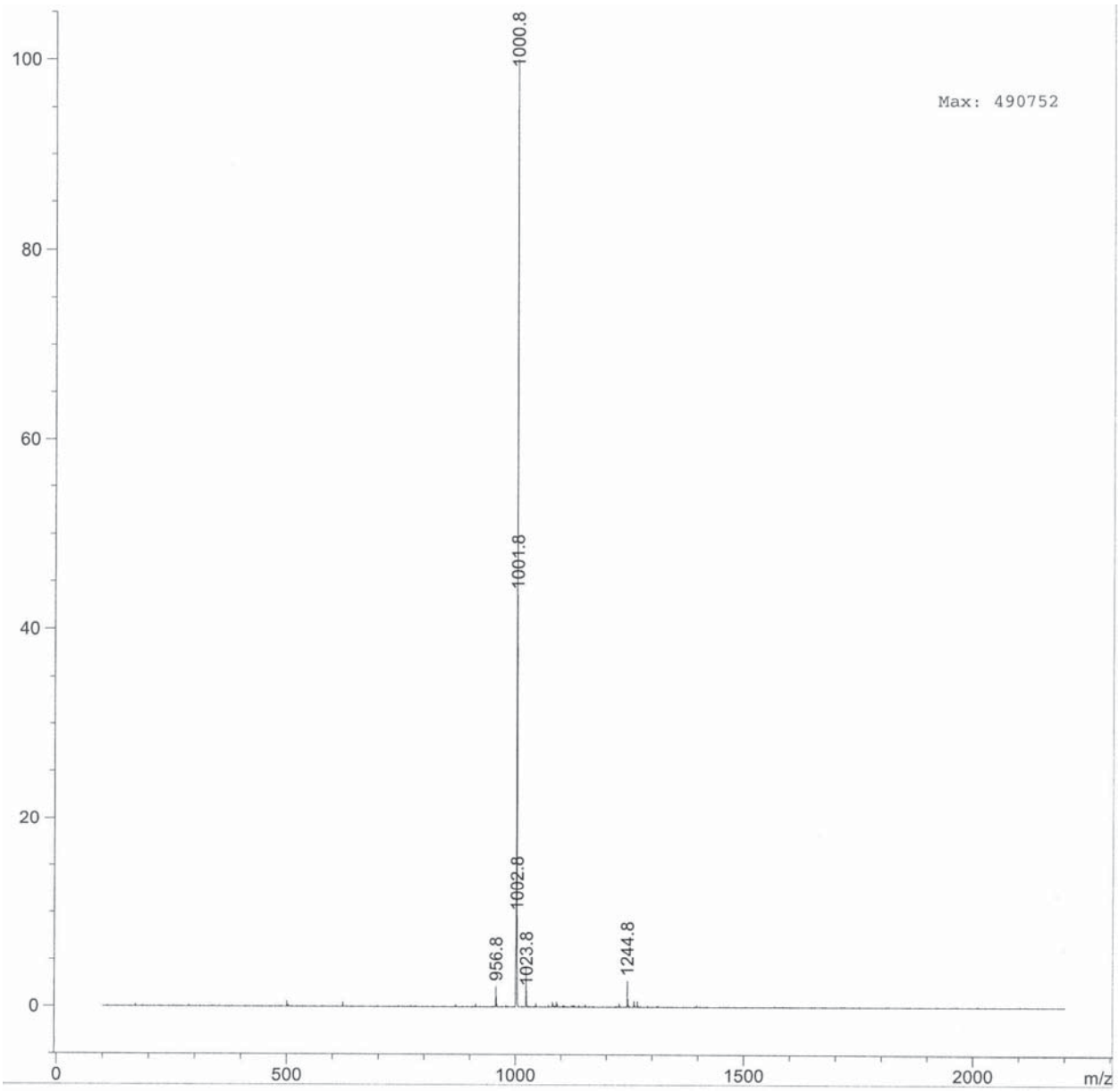

MS of RfNTA

References

(1) Falck, J. R.; Yu, J.; Cho, H.-S. *Tetrahedron Lett.* **1994**, *35*, 5997-6000.

(2) Duffy, D. C.; McDonald, J. C.; Schueller, O. J. A.; Whitesides, G. M. *Anal. Chem.* **1998**, *70*, 4974-4984.

(3) Roach, L. S.; Song, H.; Ismagilov, R. F. *Anal. Chem.* **2005**, *77*, 785-796.

(4) Seiffert, S.; Oppermann, W. *J. Microsc.-Oxf.* **2005**, *220*, 20-30.

(5) Li, L.; Mustafi, D.; Fu, Q.; Tereshko, V.; Chen, D. L. L.; Tice, J. D.; Ismagilov, R. F. *Proc. Natl. Acad. Sci. U. S. A.* **2006**, *103*, 19243-19248.

(6) Otwinowski, Z.; Minor, W. In *Macromolecular Crystallography, Pt A*; ACADEMIC PRESS INC: San Diego, 1997; Vol. 276, pp 307-326.